Diblock Copolymers Containing Metal Complexes in the Side Chain of One Block

Khaled A. Aamer, Wim H. de Jeu, and Gregory N. Tew*

Department of Polymer Science and Engineering, University of Massachusetts, Amherst, 120 Governors Drive, Amherst, Massachusetts 01003

Received July 10, 2007; Revised Manuscript Received December 11, 2007

ABSTRACT: The synthesis of novel block copolymers with metal complexes in the side chain of the polymer and their bulk self-assembly are described. Atom transfer radical polymerization plus postpolymerization chemistry were used to synthesize these novel diblock and four-arm star diblock copolymers. One block was functionalized with an asymmetric ruthenium(II) bisterpyridine complex containing a C_{16} alkyl chain in the 4′ position. ^{1}H NMR and FT-IR were used to monitor the postpolymerization chemistry, while polarized optical microscopy, small angle X-ray scattering (SAXS), and wide-angle X-ray diffraction were used to characterize the self-assembled structures. The diblock copolymer microphase separated in the bulk to form a structure-within-structure morphology "cylinders in a sea of rods" that have spacings of 38 and 5.7 nm, respectively, and the C_{16} chains were crystalline. The star copolymer was birefringent in the bulk, gave a SAXS signal corresponding to 38 nm, and had crystalline C_{16} side chains; however, no evidence for structure-within-structure could be found in the SAXS experiments. This could be due to slow relaxation times, since the molecular weight was three times larger than the linear diblock copolymer, or frustrated packing due to the star architecture.

Introduction

Noncovalent interactions are the tools that direct different molecular segments to self-assemble and include weak and strong metal−ligand complexation, hydrogen bonding, $\pi-\pi$ stacking, electrostatic forces, hydrophilic−hydrophobic interactions, and van der Waals forces.[1] Despite the great successes over the past two decades in assembling small molecules, many of the rules for organizing molecular structures are still missing.[2] Beyond this is an even greater challenge, which is to understand the manifestation of "supramolecular chemistry functional units" when they are built into macromolecules. Combining of the precision of modern organic polymer chemistry with the rich functionality of metal ions appears to be an extremely attractive and versatile approach to generating novel materials.

In the past decade, metal−ligand coordination has attracted the attention of numerous research groups.[3−11] Within the context of macromolecules, three major approaches have been followed to incorporate metal−ligand complexes into polymers that depend on the location of the metal complexes. These approaches include metal complexes in the backbone of the polymer known as coordination polymers,[12] metal complexes at the chain ends as a mean to assemble either longer chains or prepare multiblock and star polymers,[4] and metal complexes in the side chain.[5,12,13]

While great effort has been spent synthesizing these novel macromolecules with metal complexes at precise locations, in general, studies focused on the self-assembly of metal-complexes in the side chain of polymers has been quite limited. Some reports have described the assembly in solution, but very few have examined the solid-state order. A notable exception are the supramolecular systems based on bottlebrush-like structures studied by Ikkala and ten Brinke.[14,15] These materials, which take advantage of the pyridine ring in the poly(vinyl pyridine) block, are not side chain containing metal complex polymers per say but do utilize supramolecular interactions that generate a variety of ordered structures including "order-within-order" morphologies.[16−27]

The synthesis of supramolecular polymers with defined architectures requires well controlled polymerization methodology. Controlled free radical polymerization techniques including atom transfer radical polymerization (ATRP), nitroxide mediated polymerization (NMP), and reversible fragmentation−addition free radical chain transfer polymerization (RAFT) are suitable methods for this task. We and others have applied theses methods either with terpyridine (terpy) as the free ligand or in the form of metal complexes.[3,28−37] In most of the previous work, the polymers synthesized lacked control over architecture and, most importantly, the composition of either the terpy ligand or the metal complex. As a result, we have explored several methods to generate polymers with control over the architecture and incorporation of terpy.[28−33,38]

Here, we extend our methods to linear and four-arm star diblock copolymers in which the metal complexes are confined to one of the two blocks. We use ATRP to obtain well characterized polymers based on poly(styrene-*b*-*tert*-butylacrylate), p(S-*b*-*t*BA), followed by deprotection of the *tert*-butyl groups to generate an acrylic acid block and subsequent functionalization with an amine containing metal complex to form an amide bond. The metal complex is an asymmetric ruthenium(II) bisterpyridine complex in which one terypyridine contains a C_{16} alkyl chain in the 4′ position and the other contains 4′-C_5 short alkyl chain linker and is attached to the polymer backbone through an amide bond. ^{1}H NMR and FT-IR were used to monitor the postpolymerization chemistry, while polarized optical microscopy, SAXS, and WAXD were used to characterize the self-assembled structures. The diblock copolymer microphase separated into a "cylinders in a sea of rods" morphology with spacings of 38 and 5.7 nm, respectively. The C_{16} side chains of this diblock and the four-arm star were crystalline. The star copolymer was birefringent in the bulk and gave a SAXS signal corresponding to 38 nm; however, no

* To whom correspondence should be addressed. E-mail: tew@mail.pse.umass.edu.

10.1021/ma071531b CCC: $40.75
Published on Web 02/20/2008

Scheme 1. Synthesis of Linear Diblock Copolymers 6 and 7

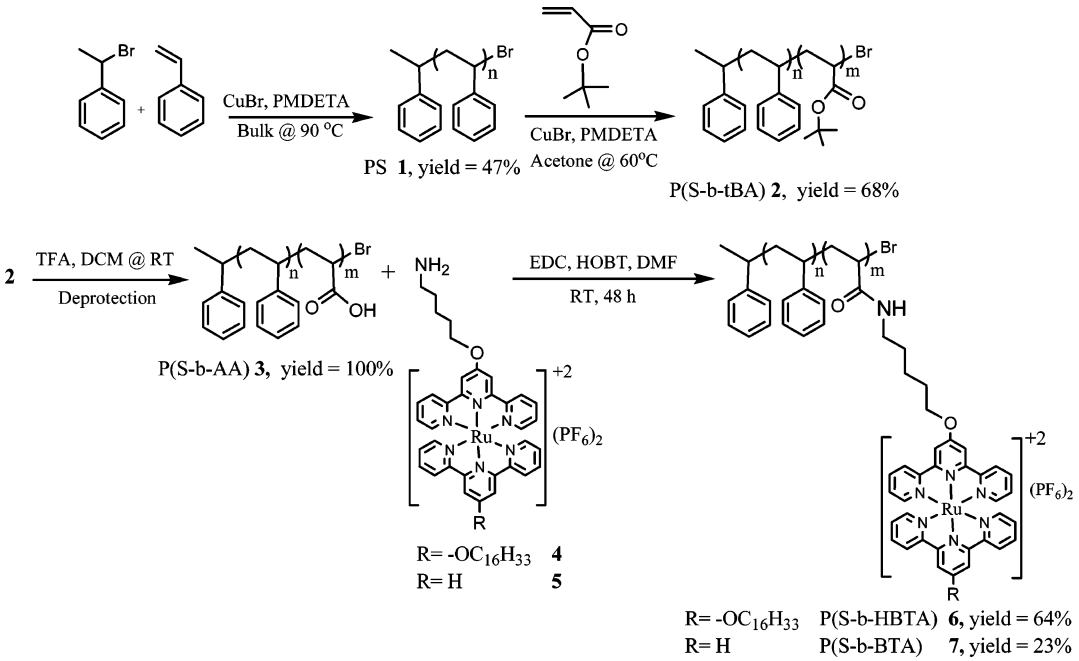

evidence for structure-within-structure morphologies could be found. The ability of these metal complex functionalized polymers to self-assemble into hierarchical structures expands the toolkit of structures with such order and begins to combine highly functionalized polymers with multiscale assembly.

Results and Discussion

Synthesis. Polymers containing metal complexes in their side chains have historically suffered from relatively limited characterization, but this has begun to change in the past few years as more sophisticated synthetic methods and improved access to analytical instrumentation have been employed by researchers in this area. Block copolymers, in which the metal complex is confined to one of the blocks, have received little attention despite the opportunities to couple rich functionality with the diverse morphologies of block copolymers. These materials are likely to have a host of interesting properties including lyotropic liquid crystallinity, unique self-assembly, controllable optical properties, and the ability to microphase separate into ordered nanostructures, which confines the metal complex chemistry, and can be manipulated with the well-known processes used in traditional block copolymers. In order to access these various properties, which are influenced by molecular weight (MW), polydispersity index (PDI), and chemical composition, synthetic routes to these structures must be accomplished.

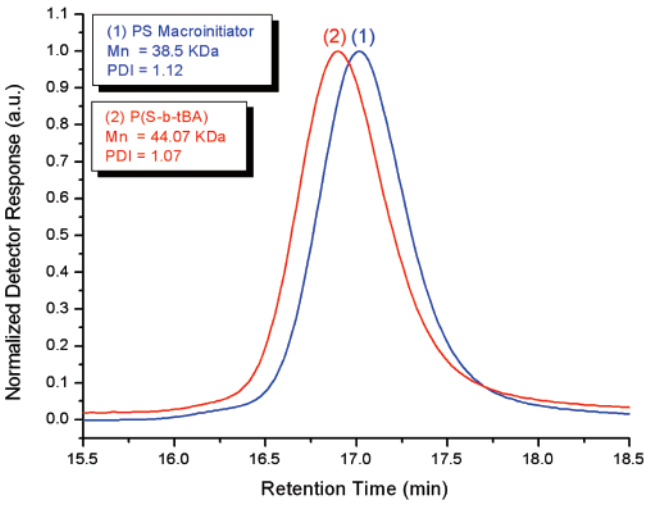

Figure 1. Overlaid chromatograms of **1** and **2** shown in Scheme 1.

Over the past few years, we have reported a number of synthetic strategies to yield well-defined polymer architectures including block copolymers with the metal ligand confined to one of the blocks. Here we take advantage of one of these approaches to prepare block and four-arm star copolymers. Scheme 1 outlines the approach to p(S-*b*-HBTA) and p(S-*b*-BTA) diblock copolymers, **6** and **7**, respectively. These two linear block copolymers different only in the 4′-terpyridine substituent which is either unsubstituted (BTA) or a C_{16} alkyl chain (HBTA). We have previously shown that the C_{16} hydrocarbon is an essential component for inducing order within the homopolymers of these materials.[29] The new diblock copolymers shown in Scheme 1 are based on styrene and *tert*-butylacrylate (*t*BA) monomers and were synthesized by ATRP.[29,39,40] Figure 1 shows the GPC chromatogram for both the PS macroinitiator, **1**, and the diblock copolymer, **2**. Deprotection of the p(*t*BA) block using trifluoroacetic acid (TFA) generates the poly(acrylic acid) function, which was then coupled with an amine functionalized $[Ru(terpy)_2]^{2+}$ complex, **4** or **5**, via standard peptide chemistry to generate the corresponding diblock copolymers **6** and **7**. The inability of terpy functionalized polymers to elute from GPC columns is well documented; terpy molecules (chelating pyridines) have high affinity to adsorb to the GPC column stationary phase which are hard to desorb. This interaction eventually leads to the clogging of the GPC column and subsequent removal from service.[28−30,41] This synthetic approach has proven to be extremely versatile in generating block copolymers and, as an example, four-arm star copolymers were prepared to further evaluate this approach.

As shown in Scheme 2, the four-arm star synthesis began by reacting pentaerythriytol with 2-bromoisobutyryl bromide to provide the four-arm ATRP initiator, $PEBr_4$. Styrene was polymerized using $PEBr_4$, CuBr, and bipyridine to give the polystyrene macroinitiator PS_4, **9**, with $M_n = 41.3$ kDa and PDI = 1.13 by GPC as shown in Figure 2. The PS_4 star nature was

Scheme 2. Synthesis of p(S-*b*-HBTA), 12, Star Diblock Copolymer

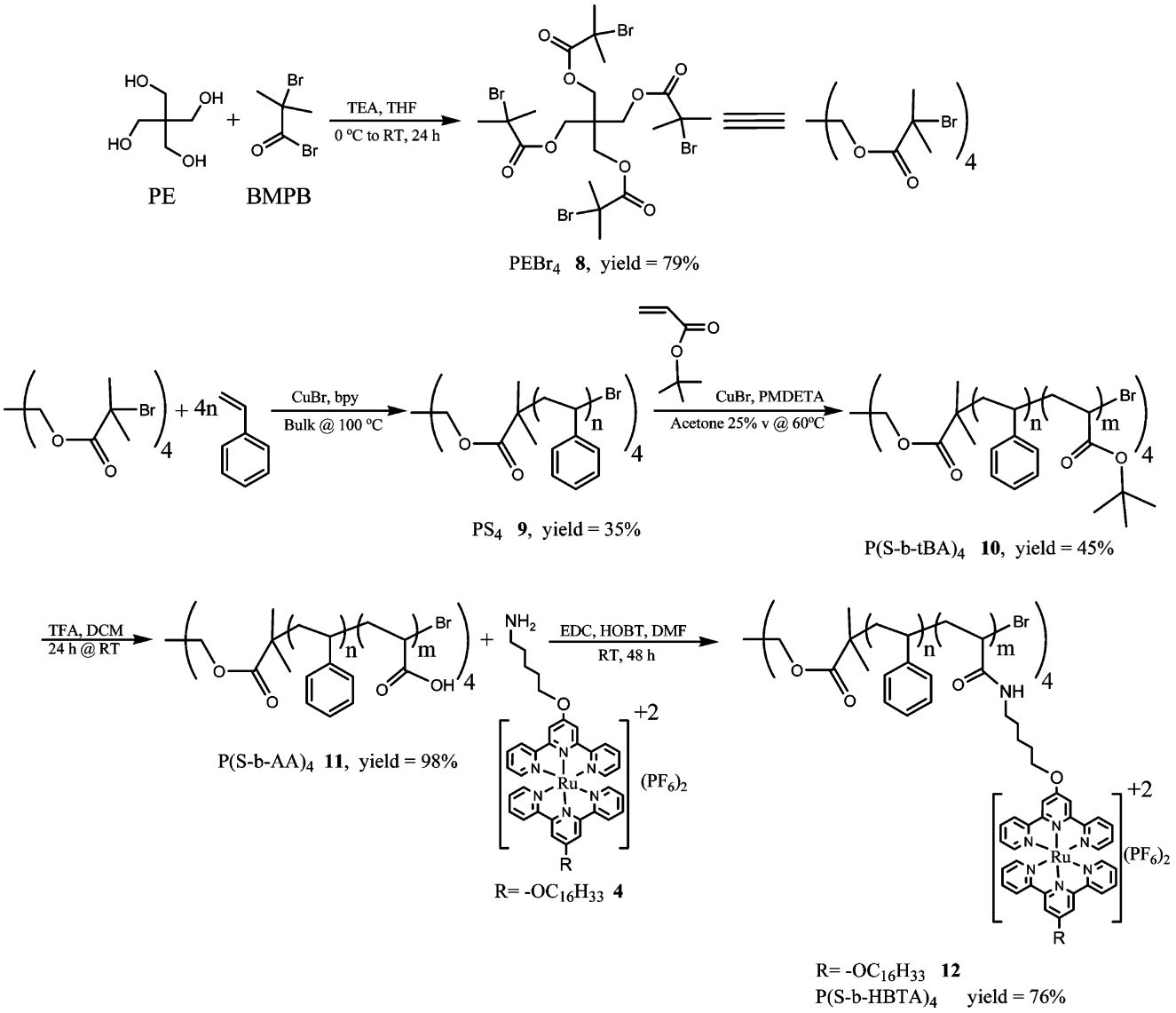

confirmed by hydrolysis of the ester bonds in the core to liberate linear polystyrene chains that were characterized by GPC to give M_n = 13.3 kDa and PDI = 1.19 (see Figure 2). From this M_n, one might have expected the M_n of the four-arm star to be around 53 kDa; however, GPC measurements indicated the four-arm star's M_n to be lower by approximately 30%. The apparent inconsistency in M_n was due to the use of linear PS GPC standards. The star polymer has a lower hydrodynamic size compared to the linear chains of the same M_n as a result of confinement by the core.[42]

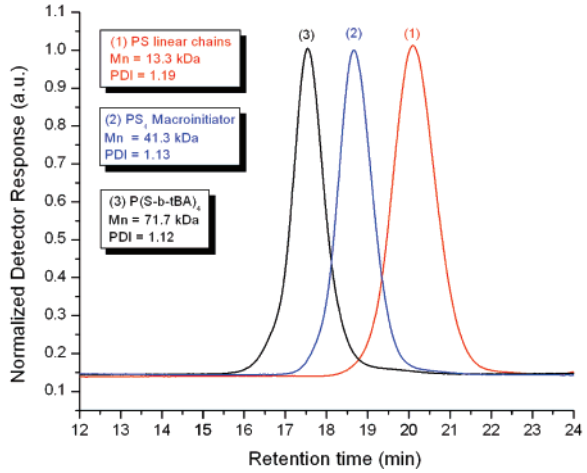

Figure 2. Overlaid GPC chromatograms of **9**, **10**, and the linear PS chains generated from cleavage of the four-arm star.

After confirmation that **9** was a four-arm star, this macroinitiator was used to polymerize *t*BA giving p(S-*b*-tBA)$_4$ star polymer, **10** (see Figure 2). With the same protocol as described in Scheme 1, the *t*BA block was deprotected and the resulting poly(acrylic acid) block was coupled with the C_{16} alkyl containing amine functionalized $[Ru(terpy)_2]^{2+}$ complex, **4**, to yield the star polymer p(S-*b*-HBTA)$_4$, **12**. Table 1 summarizes the molecular weight characterization data for the terpy functionalized copolymers p(S-*b*-HBTA) **6**, p(S-*b*-BTA) **7**, and p(S-*b*-HBTA)$_4$ **12**. The M_n values reported in Table 1 were calculated from the degree of polymerization (DP) of the parent block copolymer, p(S-*b*-*t*BA) or p(S-*b*-*t*BA)$_4$, the PDI was taken directly from that of the p(S-*b*-*t*BA) shown in Figures 1 and 2, and the fraction of PS, f_{PS}, was calculated from the DP and corresponding M_n.

To generate metal complex containing block copolymers using this approach, the critical steps in the synthetic strategy are the postpolymerization deprotection and the amide bond coupling. As we have previously reported, ^{1}H NMR and FT-IR

Table 1. Molecular Weight Characterization of Linear p(S-*b*-HBTA), 6, p(S-*b*-BTA) 7, and p(S-*b*-HBTA)$_4$, 12 Copolymers

polymer	M_n[a] × 10^3	PDI[b]	f_{PS} (wt %)
p(S-*b*-HBTA), **6**	92.4	1.07	41.67
p(S-*b*-BTA), **7**	82.1	1.07	46.91
p(S-*b*-HBTA)$_4$, **12**	299.0	1.12	17.83

[a] M_n values are calculated using monomer M_w and $\overline{DP}$ of p(*t*BA) from GPC measurements. [b] PDI is based on the polydispersity of p(S-*b*- *t*BA) and p(S-*b*-*t*BA)$_4$ protected polymers. M_n & f_{PS} are determined from GPC (THF) molecular weight measurements vs PS linear standards and ^{1}H NMR data.

are valuable techniques to monitor the *t*BA proton signals and the *t*BA carbonyl group's vibrational frequencies, separately.[29,30,32] From the ^{1}H NMR spectra, the *t*BA proton signals at 1.5 ppm disappeared following treatment with TFA; however, there was overlapping of the polymer backbone protons in this region making the analysis complicated. Fortunately, FT-IR was complementary and was used to confirm the conversion. Due to the four-arm star polymer architecture complexity in terms of steric hindrance, we expected that the postpolymerization chemistry would be of low conversion, but this was untrue, and the FT-IR data for this molecule is shown in Figure 3. The vibrational frequencies of the carbonyl shift from 1729 cm^{-1} in the *t*BA block to 1717 cm^{-1} after treatment with TFA, as can be expected for the conversion of an ester to a carboxylic acid. Unfortunately, the broad acid signal and relatively small shift still caused overlapping of the signals. However, once the acid functionalities are converted to the amide, the carbonyl shifts to even lower wavenumber at 1616 cm^{-1}. This allowed us to monitor both the original ester stretch at 1729 cm^{-1} and the acid carbonyl at 1717 cm^{-1}. From Figure 3, it is clear that very little ester or acid functionality remains present in the final copolymer, **12**. Based on ^{1}H NMR (see Supporting Information) and FT-IR, the postpolymerization conversion is greater than 95%.

Supramolecular Organization. With the diblock copolymers synthesized and characterized, their self-ordering properties were studied in concentrated solutions and bulk films. The diblock copolymer **6** containing the C_{16} functionalized metal complex block showed birefringence by polarized optical microscopy (POM) both in 15 wt % chloroform solution and in bulk. This is consistent with the previously reported metal complex containing homopolymer which formed a lyotropic liquid crystalline phase at 8 wt % in chloroform.[29] Panels a and b of Figure 4 show the room-temperature birefringence of a 100 μm thick film and a 15 wt % chloroform solution, respectively. The thin film birefringence was maintained during the entire heating and cooling cycle from 25 to 240 °C at 10 °C/minute, indicating that the bulk material remained organized over this whole temperature window. Likewise, the star copolymer **12** formed birefringent thin films at room temperature as shown in Figure 4c; however, no solution birefringence could be obtained for **12** due to limited solubility in chloroform.

Previously, we proposed that the metal complex containing homopolymer behaved as a rigid-rod-like molecule due to the increase in persistence length generated by the metal complex.[29] This was based on a number of observations, in which the polymer structure could be visualized as a polyelectrolyte−surfactant stoichiometric complex where $[Ru(terpy)_2]^{2+}$ acts as the ionic head group and the C_{16} alkyl chain acts as the hydrophobic tail grafted from the flexible polyacrylamide backbone. From the theory of these systems,[43] the flexible linear polyelectrolyte transforms to a lyotropic liquid crystal upon complexation with surfactants in good solvents for the surfactant tail. This behavior is attributed to the enhancement of the polymer persistent length of the resultant bottle-brush-like polymer. The steric repulsion from the excluded volume interactions among the surfactant tails in solution renders the flexible polymer chains stiff, forming a rodlike object prone to self-assemble.

Coupling the flexible PS block onto one end of the metal complex containing homopolymer, to produce a diblock copolymer, should generate a rod−coil architecture, and these are well known to self-assemble.[44−47] These copolymers, **6** and **12**, appear to carry the liquid crystalline properties of the rod block as evidenced from the birefringent thin films. The lyotropic behavior of **6** is also consistent with expectations, and, not surprisingly, the concentration needed to observe lyotropic behavior was slightly higher at 15 wt % for the rod−coil, **6**, than for the homopolymer (8 wt %) since the coil would not be expected to strongly induce order in this solution.[29]

Hierarchical Self-Assembly. First, consider the linear diblock copolymers for which the bulk ordering was studied by SAXS. Samples were prepared by compression between parallel plates and subsequently passing between two rollers, all at 235 °C. Figure 5 shows two different sets of SAXS data collected from

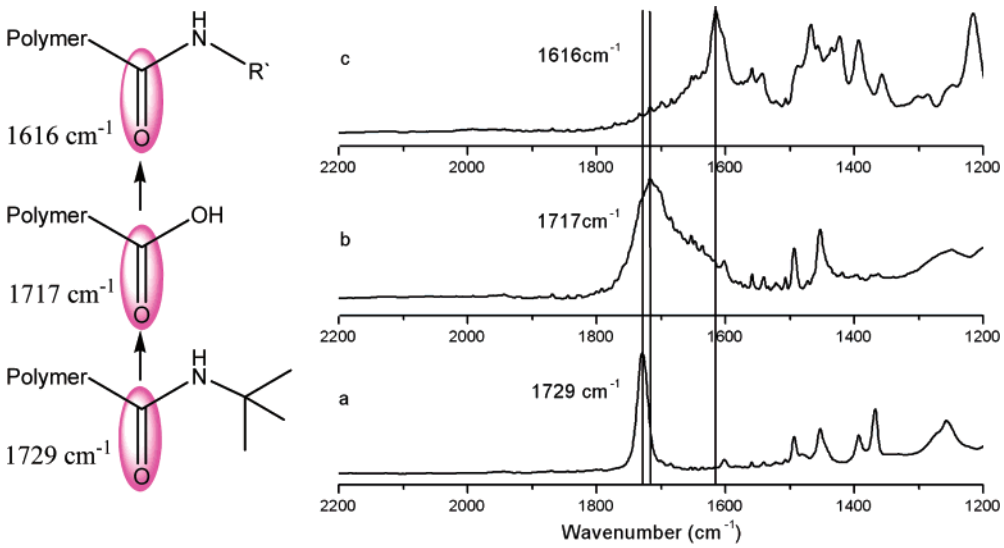

Figure 3. FT-IR stacked spectra of (a) p(S-*b*-*t*BA)$_4$, **10**, (b) p(S-*b*-AA)$_4$, **11**, and (c) p(S-*b*-HBTA)$_4$, **12** diblock copolymers from 2200 to 1200 cm^{-1}.

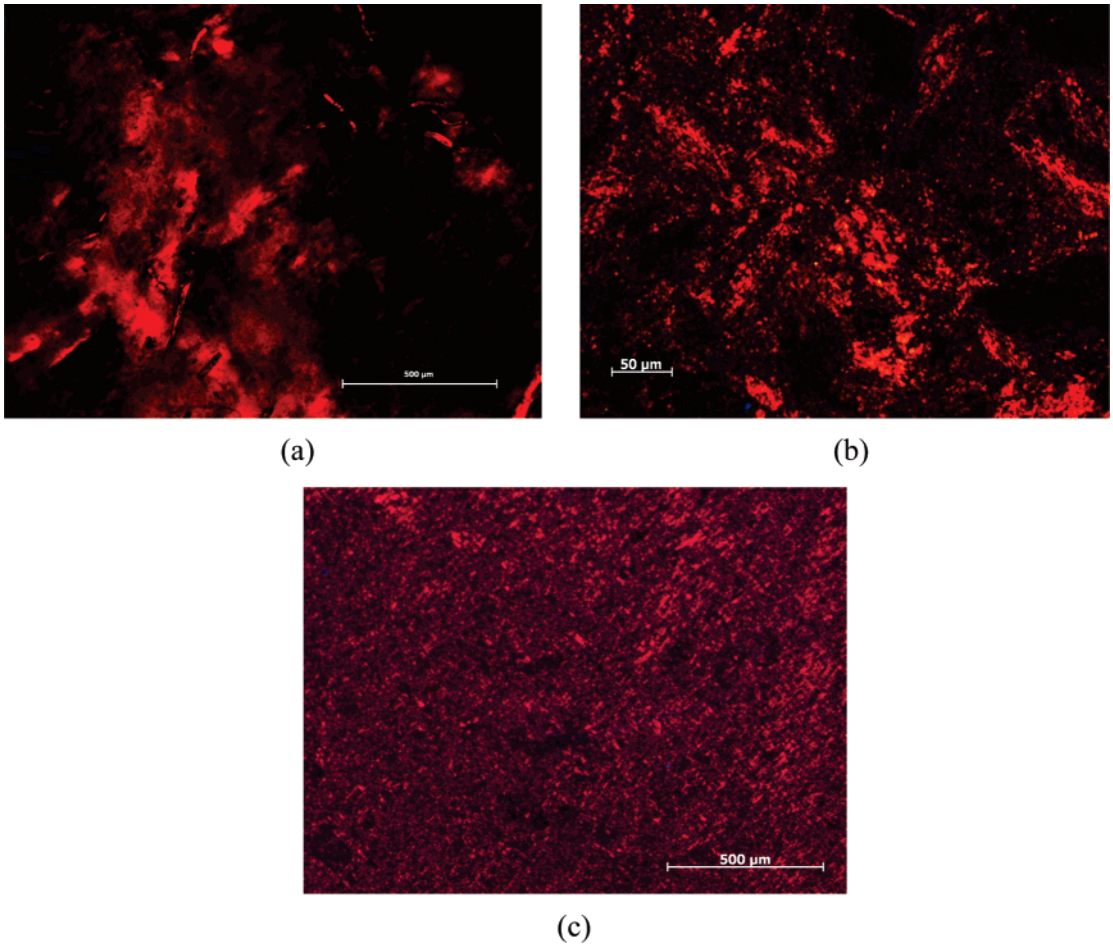

Figure 4. Polarized optical microscopy micrographs of (a) a sheared 100 μm thick film of **6,** (b) a 15 wt % solution of **6** in chloroform, and (c) a sheared 100 μm thick film of **12**. All images were taken at RT.

a sample of **6** in which the X-ray beam is either perpendicular to the *xy* plane or to the *zy* plane of the sample as defined by the image shown at the top of Figure 5. The SAXS pattern collected perpendicular to the *xy* plane is essentially isotropic (see Figure 5a) and contains two halos. From the 1-D picture of Figure 5b, obtained by full azimuthal integration of Figure 5a, we obtain periods corresponding to ~38 and 5.7 nm, respectively. The peak corresponding to the long spacing is strongly broadened at the high q side. A reasonable guess of the position of a possible second peak would be 0.30−0.32 nm^{-1}, which is close to $\sqrt{3}$ times the fundamental spacing. However, this estimate is not accurate enough to conclude ambiguously a hexagonal block morphology. Based on previous work, the 5.7 nm period is consistent with the spacing observed for the metal complex containing block. Hence, it can be attributed to small aligned cylindrical regions along the z axis (parallel to the block interfaces). To explain the observed isotropy, we must assume that these domains are not correlated and azimuthally randomly distributed. The broad background provides evidence for considerable disorder in the orientations as well.

Rotating the sample over 90°, so that the X-ray beam is parallel to the film, results in the strongly oriented pattern of Figure 5c. Two intense arcs are observed, symmetric along the q_z direction. From the 1-D plot of Figure 5d, now constructed by azimuthal integration over ±30° along the preferred direction, we find that these have almost exactly a ratio $1:\sqrt{3}$. Both peaks show a clear second harmonic at relative ratios of 2 and $2\sqrt{3}$, indicating a rather well ordered hexagonal structure parallel to the z axis. The origin of the "intensity edge" between the positions of the second and third harmonic of the fundamental is not clear at this moment.

The 5.7 nm spacing returns in Figures 5c and 5d but only marginally. In Figure 5d, a broad hump is seen between 0.7 and 1.2 nm^{-1} but appreciably weaker than in Figure 5b. Upon full azimuthal integration, its intensity increases, indicating much less pronounced orientational ordering than that for the longer period. This confirms the earlier proposition of considerable disorder of the metal complex rods.

The overall observations are consistent with microphase separation of the two blocks into hexagonally ordered cylinders, with PS expected to be the minority phase. The PS cylinders are well oriented parallel to the z axis, but in domains that are uncorrelated, to give the isotropic picture of Figure 5a. The much smaller metal complex rods have a tendency to orient in the same direction but only to a limited degree. We speculate that the complex rods orient mainly in the neighborhood of the block interfaces and are more randomly distributed in the rest of the system.

A model can be constructed for the orientation of the diblock hexagonal cylinder interfaces as well as for the pHBTA rods. To account for the hexagonal block morphology, we have to assume that the 42 wt % PS block of the p(S-*b*-HBTA) diblock copolymer translates into an increased asymmetry for the volume fractions, once the densities are take into account (unknown for HBTA). Moreover, as we have shown previously,[29] the pHBTA homopolymer self-assembles into hexagonally organized columnar rods with a long period of 5.1 nm in the bulk.

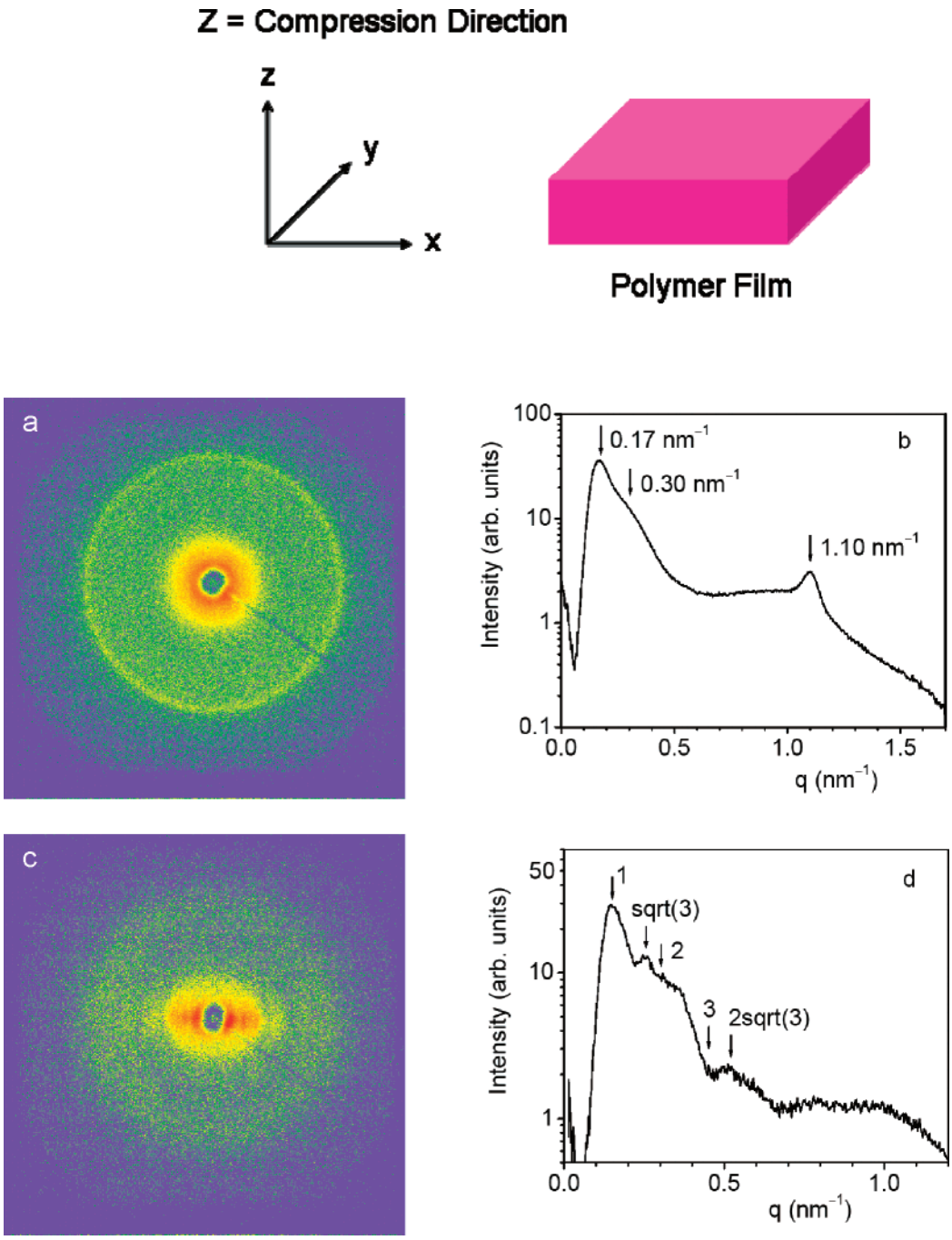

Figure 5. SAXS patterns from the diblock copolymer **6**. (a) 2-D SAXS pattern with the X-ray beam perpendicular to the *xy* direction showing two scattering halos corresponding to 38.1 and 5.7 nm, respectively. (b) 1-D SAXS pattern obtained by full azimuthal integration of panel a. (c) 2-D SAXS pattern with the X-ray beam perpendicular to the *zy* direction. (d) 1-D SAXS pattern obtained by azimuthal integration over ±30° with respect to the preferred direction in panel c.

The morphology was expected to be preserved in the diblock system, and this assumption is substantiated by the scattering signal corresponding to 5.7 nm. The SAXS pattern shows that the diblock copolymer microphase separates into an ordered material with two different length scales. The (poorly oriented) hexagonally packed rods represented by the 5.7 nm long period and the well oriented cylinders of the alternating PS and pHBTA blocks with a period of about 38 nm. This hierarchical cylinders in a sea of rods morphology is a direct result of the molecular design. Such a structure requires two critical elements to be included in the block architecture which promote microphase separation into PS and pHBTA domains that pack into hexagonal cylinders and additionally the rodlike nature of the constituting elements within the pHBTA block.

The star copolymer, **12**, was studied in the same manner as the diblock copolymer. Figure 6 shows that the 1-D SAXS pattern for this film gives two broad reflections corresponding to a long period of about 38 nm and a ratio 1:$\sqrt{3}$. All efforts to orient the material or improve the long-range order using oscillatory shear did not lead to more informative SAXS patterns. The M_n of this sample is more than three times larger than the linear diblock copolymer, which might increase the time for annealing. The fundamental spacing and the assumed hexagonal symmetry are very similar to **6**, even though the star polymer contains only 18 wt % PS. When compared to a conventional block copolymer phase diagram, one would anticipate a spherical morphology with PS spheres embedded in a matrix of pHBTA rods. However, with the limited number

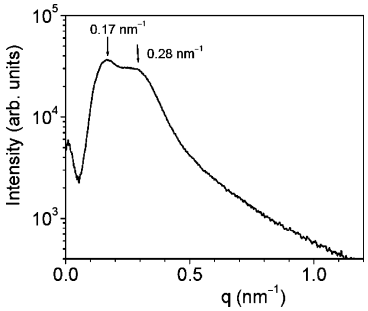

Figure 6. SAXS pattern for p(S-*b*-HBTA)$_4$ star copolymer, **12**, for the bulk sample.

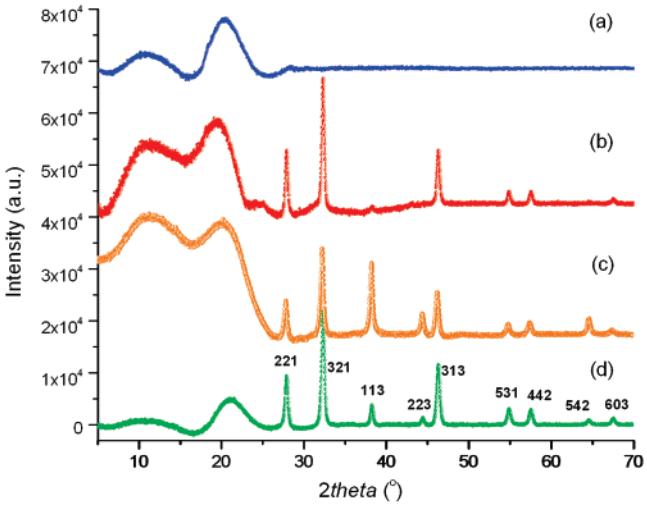

Figure 7. Wide angle powder X-ray diffraction pattern data for the diblock copolymers (a) **7** with no C_{16} groups, (b) **6**, the linear diblock, (c) **12**, the star, and (d) the pHBTA homopolymer.

of reflections, a phase morphology cannot be definitely assigned. In addition the 5.7 nm signal corresponding to packing of the pHBTA rods is not observed. This may be attributed to frustration imposed by the four-arm core which constrains the pHBTA domains.

Side Chain Crystallinity. One of the interesting features of the previously reported homopolymer was the presence of crystallinity within the C_{16} alkyl chains. To characterize the presence or absence of crystallinity here, the two block copolymers, **6** and **12**, were studied by WAXD. The WAXD patterns (Figure 7) show that both the diblock and the star copolymers possess crystalline order as indicated by the strong scattering signals between 28 and 70°. Comparison of the WAXD patterns of **6**, **7**, and **12** shows that **7**, which does not contain the C_{16} group, lacks all the crystalline peaks above 25° observed for both **6** and **12**. Figure 7 also contains the WAXD pattern of the pHBTA homopolymer alone to confirm that the C_{16} alkyl chains are responsible for this crystalline behavior. Fitting the sharp signals provided a tetragonal unit cell with unit cell parameters of $a = b = 10.02$ Å, $c = 7.50$ Å, and $\alpha = \beta = \delta = 90°$, which match those for the pHBTA homopolymer.

Conclusions

In this report, we have demonstrated that the indirect method is a successful general method to synthesize linear and four-arm star diblock copolymers with high fidelity. Both the linear and star copolymers containing $[Ru(terpy)_2]^{2+}$ with C_{16} alkyl chains formed ordered materials in the bulk. Self-assembly of the p(S-*b*-HBTA) diblock led to the hierarchical "cylinders in a sea of rods" morphology which showed nanostructured order with two different length scales at 5.7 and 38 nm, respectively. The pHBTA cylinders have a crystalline outer shell of the C_{16} chains, and this structure is preserved in the diblock and star copolymers. Learning to program self-assembly into functional materials remains a very important goal, and the present systems outline methods to create hierarchically ordered metal complex containing polymers.

Experimental Section

Materials, Measurements, and Sample Preparation. Polymer synthesis and molecular characterization data are provided in the Supporting Information. Here we describe the major sample preparations and methods used.

FT-IR Spectroscopy. The FT-IR measurements were performed at room temperature on a Perkin-Elmer FT-IR Spectrometer, Spectrum 2000. Polymers were dissolved either in DCM, or in THF with a drop of water or methanol and casted over ZnSe pellets and then allowed to dry at room temperature before measurements.

UV−vis Spectroscopy. UV−vis spectroscopy measurements were recorded using a Lambda 25 Perkin-Elmer UV WinLab 5.1.4.0630/ Lambda25 1.24 Lambda 2 series spectrophotometer. The instrument was calibrated against spectroscopic grade acetonitrile solvent.

Polarized Optical Light Microscopy (POM). The lyotropic liquid crystal birefringence patterns were examined at room temperature via POM combined with a Linkam Scientific Instrument hot stage LTS350, Axioskop 40, Zeiss. The images were captured using an insight digital camera, AxioCam MRc5, combined with AxioVision Vs40AC v4.4.0.0 software. The polymer solutions (9−15 wt %) were prepared in $CHCl_3$ and sheared between glass cover slides. For thin films, see X-ray scattering section.

Thermal Analysis. The onset of polymer thermal degradation (T_{deg}) and the degradation profile were recorded using thermal gravimetric analysis (TGA) instrument 2050 TGA V5.3C Module. TGA was performed under a stream of N_2 gas. The temperature program that was used allowed the temperature to increase at 10 °C/min between 30 and 1000 °C. Differential Scanning Calorimetry (DSC) was used to measure the glass transition temperature of the polymers (T_g). The T_g's were recorded under a stream of N_2 gas using a 2910 MDSC V4.4E Module modulated DSC. An endothermic hysteresis program allowed the samples to be cooled down at 2 °C/min starting at 240 °C and going down to −50 °C and then heated at 40 °C/min up to 240 °C. Two cooling and heating cycles were recorded, and only the T_g value from the second cycle is reported. Sample size ranged from 5 to 7 mg before being used, and the samples were sealed in aluminum pans.

The onset of thermal degradation T_{deg} for both systems was around 260 °C and is similar to the values reported by Frazer for $[Ru(bpyPLA_2)_3]^{2+}$ star polymers.[40] The glass transition temperature T_g for the metal complex containing block could not be observed for both p(S-*b*-HBTA) and p(S-*b*-HBTA)$_4$ by the conventional DSC method in the range −50 to 240 °C. However, endothermic hysteresis experiments are known to make the T_g transition more pronounced.[28] In this experiment, the sample is slowly cooled from a high temperature (240 °C) and then heated rapidly across the region in which the glass transition in expected. By employing this approach, the T_g of p(S-*b*-HBTA) **6** was determined to be 113 °C for the PS block and 165 °C for the metal complex containing block while that determined for the star polymer p(S-*b*-HBTA)$_4$ **12** was 110 °C for the PS block and 179 °C for the metal complex containing block.

X-ray Scattering. Small-angle and wide-angle X-ray diffraction studies were performed using an instrument from the Molecular Metrology Inc., equipped with a focusing multilayer monochromator (Osmic MaxFlux) at a wavelength $\lambda = 1.54$ Å. The beam was further defined and collimated by two pinholes and a third one acting as an antiscattering slit. For the small-angle detection, a 2-D multiwire detector was set at a sample−detector distance of 1.5 m. Silver behenate ($d_{001} = 5.838$ nm) was used for angular calibration. Thin films were prepared by solution casting the polymer into teflon molds. Once dried, the films were removed and compressed between

parallel plates at 30 000 lbs/in at 235 °C for 5 h. Following this compression, the film was passed through two heated rollers, also at 235 °C, to orient the microdomains.

Wide-Angle X-ray Powder Diffraction (WAXD). Patterns were recorded using X'Pert pro PANalytical operated at 45 kV and 45 mA using Cu Kα radiation at a wavelength $\lambda = 1.54$ Å. The diffraction pattern was acquired between 2θ angle of 1.5 and 70° using X'celerator detector. The data were analyzed and the unit cell parameters were obtained using powder X-ray data analysis program.

Acknowledgment. We thank the ARO Young Investigator and PECASE programs for generous support of this work as well as the Materials Research Science and Engineering Center program of the National Science Foundation under Award (DMR 9400488). G.N.T. thanks the ONR Young Investigator, NSF-CAREER, 3M Nontenured faculty grant and Dupont Young Faculty Award programs for support.

Supporting Information Available: Polymer synthesis details and molecular characterization data. This material is available free of charge via the Internet at http://pubs.acs.org.

References and Notes

(1) Lehn, J.-M. *Supramolecular Chemistry: Concepts and Perspectives*; Wiley-VCH: New York, 1995.
(2) Stupp, S. I.; Keser, M.; Tew, G. N. *Polymer* **1998**, *39*, 4505−4508.
(3) Andreopoulou, A. K.; Kallitsis, J. K. *Eur. J. Org. Chem.* **2005**, 4448−4458.
(4) Beck, J. B.; Rowan, S. J. *J. Am. Chem. Soc.* **2003**, *125*, 13922−13923.
(5) Carlise, J. R.; Weck, M. *J. Polym. Sci., Part A: Polym. Chem.* **2004**, *42*, 2973−2984.
(6) Chen, B.; Sleiman, H. F. *Macromolecules* **2004**, *37*, 5866−5872.
(7) Dobrawa, R.; Lysetska, M.; Ballester, P.; Grune, M.; Wurthner, F. *Macromolecules* **2005**, *38*, 1315−1325.
(8) Holder, E.; Marin, V.; Meier, M. A. R.; Schubert, U. S. *Macromol. Rapid Commun.* **2004**, *25*, 1491−1496.
(9) Johnson, R. M.; Fraser, C. L. *Macromolecules* **2004**, *37*, 2718−2727.
(10) Knapton, D.; Iyer, P. K.; Rowan, S. J.; Weder, C. *Macromolecules* **2006**, *39*, 4069−4075.
(11) McAlvin, J. E.; Fraser, C. L. *Macromolecules* **1999**, *32*, 1341−1347.
(12) Kurth, D. G.; Schutte, M.; Wen, J. *Colloids Surf., A* **2002**, *198*, 633−643.
(13) Pollino, J. M.; Stubbs, L. P.; Weck, M. *J. Am. Chem. Soc.* **2004**, *126*, 563−567.
(14) Ikkala, O.; Ruokolainen, J.; Tenbrinke, G.; Torkkeli, M.; Serimaa, R. *Macromolecules* **1995**, *28*, 7088−7094.
(15) Ruokolainen, J.; Makinen, R.; Torkkeli, M.; Makela, T.; Serimaa, R.; ten Brinke, G.; Ikkala, O. *Science* **1998**, *280*, 557−560.
(16) Babin, J.; Rodriguez-Hernandez, J.; Lecommandoux, S.; Klok, H. A.; Achard, M. F. *Faraday Discuss.* **2005**, *128*, 179−192.
(17) Schlaad, H.; Kukula, H.; Smarsly, B.; Antonietti, M.; Pakula, T. *Polymer* **2002**, *43*, 5321−5328.
(18) Lecommandoux, S.; Achard, M. F.; Langenwalter, J. F.; Klok, H. A. *Macromolecules* **2001**, *34*, 9100−9111.
(19) Klok, H. A.; Langenwalter, J. F.; Lecommandoux, S. *Macromolecules* **2000**, *33*, 7819−7826.
(20) Douy, A.; Gallot, B. *Polymer* **1982**, *23*, 1039−1044.
(21) Billot, J. P.; Douy, A.; Gallot, B. *Makromol. Chem.* **1977**, *178*, 1641−1650.
(22) Perly, B.; Douy, A.; Gallot, B. *Makromol. Chem.* **1976**, *177*, 2569−2589.
(23) Billot, J. P.; Douy, A.; Gallot, B. *Makromol. Chem.* **1976**, *177*, 1889−1893.
(24) Ikkala, O.; ten Brinke, G. *Chem. Commun.* **2004**, 2131−2137.
(25) Ikkala, O.; ten Brinke, G. *Science* **2002**, *295*, 2407−2409.
(26) Ruokolainen, J.; ten Brinke, G.; Ikkala, O. *Adv. Mater.* **1999**, *11*, 777−780.
(27) Ruokolainen, J.; Saariaho, M.; Ikkala, O.; ten Brinke, G.; Thomas, E. L.; Torkkeli, M.; Serimaa, R. *Macromolecules* **1999**, *32*, 1152−1158.
(28) Aamer, K. A.; Tew, G. N. *Macromolecules* **2004**, *37*, 1990−1993.
(29) Aamer, K. A.; Tew, G. N. *Macromolecules* **2007**, *40*, 2737−2744.
(30) Aamer, K. A.; Tew, G. N. *J. Polym. Sci., Part A: Polym. Chem.* **2007**, *45*, 1109−1121.
(31) Calzia, K. J.; Tew, G. N. *Macromolecules* **2002**, *35*, 6090−6093.
(32) Shunmugam, R.; Tew, G. N. *J. Polym. Sci., Part A: Polym. Chem.* **2005**, *43*, 5831−5843.
(33) Tew, G. N.; Aamer, K.; Shunmugam, R. *Polymer* **2005**, *46*, 8440−8447.
(34) Tzanetos, N. P.; Andreopoulou, A. K.; Kallitsis, J. K. *J. Polym. Sci., Part A: Polym. Chem.* **2005**, *43*, 4838−4848.
(35) Schubert, U. S.; Hofmeier, H. *Macromol. Rapid Commun.* **2002**, *23*, 561−566.
(36) Gohy, J. F.; Lohmeijer, B. G. G.; Schubert, U. S. *Chem.—Eur. J.* **2003**, *9*, 3472−3479.
(37) Lohmeijer, B. G. G.; Schubert, U. S. *J. Polym. Sci., Part A: Polym. Chem.* **2003**, *41*, 1413−1427.
(38) Shunmugam, R.; Tew, G. N. *J. Am. Chem. Soc.* **2005**, *127*, 13567−13572.
(39) Aamer, K. A.; Tew, G. N. *Macromolecules* **2007**, *40*, 2737−2744.
(40) Matyjaszewski, K.; Xia, J. *Chem. Rev.* **2001**, *101*, 2921−2990.
(41) Meier, M. A. R.; Hofmeier, H.; Abeln, C. H.; Tziatzios, C.; Rasa, M.; Schubert, D.; Schubert, U. S. *E-Polymers* **2006**.
(42) Huang, H.-M.; Liu, I.-C.; Tsiang, R. C.-C. *Polymer* **2005**, *46*, 955−963.
(43) Fredrickson, G. H. *Macromolecules* **1993**, *26*, 2825−2831.
(44) Stupp, S. I.; Pralle, M. U.; Tew, G. N.; Li, L. M.; Sayar, M.; Zubarev, E. R. *MRS Bull.* **2000**, *25*, 42−48.
(45) Tew, G. N.; Pralle, M. U.; Stupp, S. I. *Angew. Chem., Int. Ed.* **2000**, *39*, 517−521.
(46) Tew, G. N.; Pralle, M. U.; Stupp, S. I. *J. Am. Chem. Soc.* **1999**, *121*, 9852−9866.
(47) Lee, M.; Cho, B.-K.; Zin, W.-C. *Chem. Rev.* **2001**, *101*, 3869−3892.

MA071531B